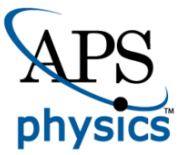

Manipulating Quantum Pathways on the Fly

Roberto Rey-de-Castro, Zaki Leghtas, and Herschel Rabitz

Phys. Rev. Lett. **110**, 223601 — Published 29 May 2013

DOI: 10.1103/PhysRevLett.110.223601

Manipulating Quantum Pathways on the Fly

Roberto Rey-de-Castro[†], Zaki Leghtas[†,‡], and Herschel Rabitz[†]

May 2, 2013

[†]Department of Chemistry, Princeton University, Princeton, New Jersey 08544, USA

[‡]INRIA Paris-Rocquencourt Domaine de Voluceau, BP105 78153 Le Chesnay Cedex, France

Abstract

The expectation value of a quantum system observable can be written as a sum over interfering pathway amplitudes. In this letter, we demonstrate for the fist time adaptive manipulation of quantum pathways using the Hamiltonian Encoding-Observable Decoding (HE-OD) technique. The principles of HE-OD are illustrated for population transfer in atomic Rubidium using shaped femtosecond laser pulses. The ability to manipulate multiple pathway amplitudes is of fundamental importance in all quantum control applications.

Controlling quantum phenomena often entails the identification of an optimal applied field which maximizes the value of an observable [1]. To meet the physical objective, the optimum field may induce advantageous constructive and destructive interferences between quantum pathways, but explicit management of the quantum pathway amplitudes is not possible through the measurement of an observable alone. Gaining control over the quantum pathway amplitudes is being pursued for fundamental reasons as well as the basis of future technologies in which the evolution of a quantum system is carefully manipulated to reach specific design goals. Here we demonstrate for the first time explicit control over pathway amplitudes through an adaptive procedure based on the novel Hamiltonian Encoding-Observable decoding (HE-OD) technique [2, 3, 4, 5, 6]. The possibility of adaptive pathway

control was recognized in the original theoretical development underlying HE-OD [2], but only recent advances [5] permitted its experimental implementation. Most importantly, this letter demonstrates that the Hamiltonian encoding in HE-OD can be made highly efficient (see sec. 1 in ref. [7]) in order to operate on the fly in real time to guide control experiments. In contrast with traditional methods for determining mechanistic information [8, 9, 10, 11, 12, 13, 14, 15, 16, 17, 18, 19], HE-OD does not require heavy post-processing of data or solving the Schrödinger equation, thereby allowing for its utilization in high-duty-cycle optimization experiments, generally with small or no changes to the laser hardware (Figure 1) available in many laboratories.

The principles of HE-OD pathway guided control are illustrated here for a gas phase sample of atomic Rb in a cell at 100 $^{\circ}C$. A laser pulse creates excitation into states $|4\rangle$ and $|5\rangle$ of Rb (see Figure 2). The final population of state $|4\rangle$ relaxes through spontaneous microwave emission to state $|O\rangle$, and then decays back to $|1\rangle$ emitting fluorescence at 421.55 nm. The latter emission was then imaged to an Ocean Optics HR-2000 (400nm) spectrometer and integrated to become the output signal $\langle O\rangle$, which is proportional to the achieved final population of state $|4\rangle$. The experiments utilized a KM-Labs Ti:sapphire femtosecond laser consisting of a Griffin oscillator and a 3 kHz Dragon amplifier. The amplified pulses had a fluence at the sample of $\sim 400\ \mu J/cm^2$ and a full width at half maximum (FWHM) of $\sim$ 40 nm centered at 783 nm corresponding to a transform-limited temporal pulse width of ~30 fs FWHM. Under these conditions laser-induced ionization of the Rb atoms is negligible (see Sec. 4 of ref. [7]). Phase modulation was performed with a 4-f configuration pulse shaper having a liquid crystal display (LCD) with 640 pixels (CRI-SLM), as shown in Figure 1. Each pixel controlled a ~0.2-nm-wide section of the spectrum, which defines the spectral resolution of our control experiments. Groups of four pixels were locked together, producing 160 parameters for optimization.

For our experimental conditions, Rb may be viewed as a five-level system with free Hamiltonian H_0 and dipole moment μ. We denote by $|k\rangle$ the eigenvector of H_0 associated to the eigenvalue ϵ_k, $k = 1, \ldots, 5$. A schematic energy level diagram specifying the allowed electronic transitions is given in Figure 2. The system state is $|\psi(t)\rangle$, and $E(t)$ is the electric field of the applied laser pulse which serves as a control. The evolution is described by $|\psi(t)\rangle = U(t)|\psi(0)\rangle$, where $|\psi(0)\rangle = |1\rangle$ and $U(t)$ satisfies

$$i\hbar \frac{d}{dt} U(t) \quad = \quad (H_0 - \mu E(t))U(t), \tag{1}$$

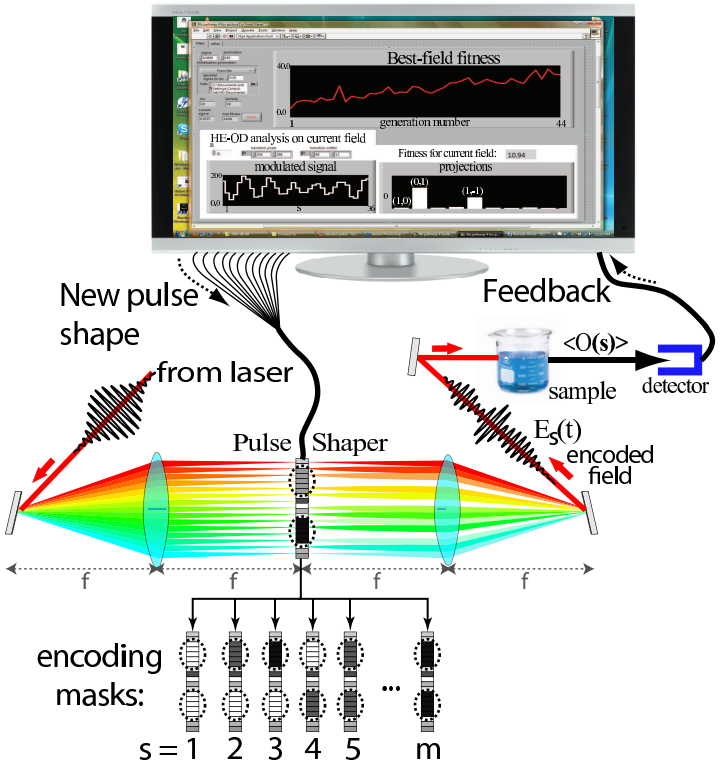

Figure 1: Setup for measuring and manipulating quantum pathways using HE-OD. A shaped laser pulse interacts with a sample, producing an output signal that is fed back to a computer. The goal is to maximize the amplitudes of particular quantum pathways while minimizing others. Information about the participating pathways is obtained through the HE-OD encoding-decoding procedure where special perturbations are introduced in the field $E(t)$ through encoding masks in the pulse shaper, and the effect of the encoded field $E_s(t)$ on the output signal is decoded to reveal the amplitudes of the various quantum pathways induced by $E(t)$. The lower part of the figure illustrates how the encoding perturbations are implemented by systematically changing the phase of the circled pixels in each mask over a sequence of m separate measurements. The extracted pathway amplitudes prescribe a cost function directing the closed-loop process to optimize a pathway-biased physical goal.

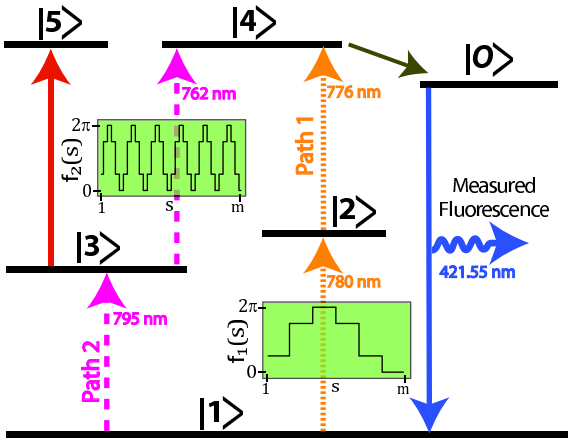

Figure 2: Energy level diagram and transitions for atomic Rb. States $|1\rangle, |2\rangle, |3\rangle, |4\rangle, |5\rangle,$ and $|O\rangle$ correspond to the levels $5S_{1/2}, 5P_{1/2}, 5P_{3/2}, 5D_{3/2}, 5D_{5/2},$ and $6P_{1/2}$, respectively. Initially only the ground state $|1\rangle$ is populated. The laser pulse excites the upper levels. After the laser pulse is over, the final population of level $|4\rangle$ decays to level $|O\rangle$ which, in turn, decays back to $|1\rangle$ emitting fluorescence at 421.55-nm. This fluorescence line is measured and taken as the signal $\langle O\rangle$, which is proportional to the final population of state $|4\rangle$. The green-background plots inserted over transitions $|1\rangle \rightarrow |2\rangle$ and $|3\rangle \rightarrow |4\rangle$ illustrate the encoding implemented over $m = 36$ measurements. In measurement s, with $s = 1, 2, \ldots, m$, the phases of the spectral components of $E(t)$ around 762 nm and 780 nm were encoded by adding in $f_1(s)$ and $f_2(s)$ to modulate path 1 (orange-dotted arrows) and path 2 (purple-dashed arrows), respectively. Level $|5\rangle$ is also populated, but it does not contribute to the measured fluorescence, and it can be omitted from the analysis as only second-order pathways are significantly involved. Not shown is the path for fluorescence at 420-nm associated with states $|4\rangle$ and $|5\rangle$.

with $U(0) = I$, where I is the identity operator. As mentioned above, the measured observable is proportional to the population in state $|4\rangle$ at a long time T after the pulse is over

$$\langle O \rangle \propto |\langle 4|U(T)|1\rangle|^2. \tag{2}$$

To understand the experiments we solve Eq. (1) using time-dependent perturbation theory in the rotating wave approximation. Neglecting terms third order in the field or higher, we get:

$$e^{i\epsilon_4 T/\hbar}\langle 4|U(T)|1\rangle = U_1 + U_2. \tag{3}$$

where,

$$U_1 = \int_0^T \mu_{42} e^{-i\omega_{42}t_2} E(t_2) \int_0^{t_2} \mu_{21} e^{-i\omega_{21}t_1} E(t_1) dt_1 dt_2 \tag{4}$$

$$U_2 = \int_0^T \mu_{43} e^{-i\omega_{43}t_2} E(t_2) \int_0^{t_2} \mu_{31} e^{-i\omega_{31}t_1} E(t_1) dt_1 dt_2 \tag{5}$$

with $\omega_{jk} = (\epsilon_j - \epsilon_k)/\hbar$, and $\mu_{jk} = \langle j|\mu|k\rangle$, for j, k = 1, 2, ..., 5. We refer to U_1 and U_2 (and their higher-order analogs) as quantum control pathway amplitudes. U_1 and U_2 are, respectively, the probability amplitudes for a Rb atom to follow the sequence of transitions: $|1\rangle \rightarrow |2\rangle \rightarrow |4\rangle$ and $|1\rangle \rightarrow |3\rangle \rightarrow |4\rangle$ and will be referred to as pathways 1 and 2. Our aim is to find fields $E(t)$ that control the relative contribution of the amplitudes U_1 and U_2 in making the overall transfer of population to state $|4\rangle$. Thus, in the experiments described here the HE-OD technique is applied on the fly to either increase or decrease the ratio $|U_1/U_2|$.

We now describe the procedure for obtaining $|U_1/U_2|$ from a sequence of measurements of the observable $\langle O \rangle$. From Eqs. (4) and (5) we see that if $\omega_0 T >> 1$, only the frequency components of $E(t)$ close to ω_{12} and ω_{24} will contribute to U_1 (resonance condition), and in the same way, only the frequency components of $E(t)$ close to ω_{13} and ω_{34} will contribute to U_2. HE-OD is performed by the addition of encoding phases to selected spectral components of $E(t)$. This is done through a sequence of m separate experiments in which the added phases are varied systematically (see Figure 1). The added phases modulate the output signal $\langle O(s) \rangle$, which is labeled by the modulation index parameter $s = 1, 2, \ldots m$. In our experiments two encoding phases were inserted into the control

field $E(t)$: phase $f_1(s)$ was added to a band $\delta\omega_1$ of spectral components of $E(t)$ around frequency ω_{21}, and $f_2(s)$ was added to another band $\delta\omega_2$ of spectral components around ω_{43}. The encoding functions $f_1(s)$ and $f_2(s)$ are explicitly given in Sec. 1 of ref. [7]. Thus, the encoded field for $s = 1, \ldots, m$ is given by

$$\begin{aligned} E_s(t) &= C_0(t)e^{i\omega_o t} + C_1(t)e^{i[\omega_{21}t + f_1(s)]} \\ &\quad + C_2(t)e^{i[\omega_{43}t + f_2(s)]} + c.c \end{aligned} \tag{6}$$

where, ω_0 is the laser carrier frequency, and $C_0(t)$, $C_1(t)$, and $C_2(t)$ are slowly-varying functions. The original field $E(t)$ is recovered by making $f_1 = f_2 = 0$ in Eq. (6). By limiting the encoding to selected portions of the absorbed spectrum around ω_{21} and ω_{43} the pathways are in general only partially encoded. Inserting Eq. (6) into Eqs. (4) and (5), and neglecting the integrals with highly oscillating (off resonant) terms gives

$$U_1(s) = U_{1ne} + U_{1e}e^{if_1(s)} \tag{7}$$

$$U_2(s) = U_{2ne} + U_{2e}e^{if_2(s)} \tag{8}$$

where, U_{1e} and U_{1ne} (U_{2e} and U_{2ne}) are the encoded and unencoded portions of pathway 1 (pathway 2), respectively. These partial amplitudes are related to U_1 and U_2 by $U_1 = U_{1ne} + U_{1e}$ and $U_2 = U_{2ne} + U_{2e}$.

Utilizing Eqs. (7) and (8) in Eqs. (3) and (2), gives

$$\begin{aligned} \langle O(s)\rangle &\propto \left|\left(U_{1ne} + U_{1e}e^{if_1(s)}\right) + \left(U_{2ne} + U_{2e}e^{if_2(s)}\right)\right|^2 \\ &\propto DC + [U_{1ne} + U_{2ne}]^* U_{1e}e^{if_1(s)} + U_{1e}U_{2e}^* e^{i[f_1(s) - f_2(s)]} + \\ &+ [U_{1ne} + U_{2ne}]^* U_{2e}e^{if_2(s)} + c.c. \end{aligned} \tag{9}$$

where, $DC = |U_{1ne} + U_{2ne}|^2 + |U_{1e}|^2 + |U_{2e}|^2$ is a constant term independent of s. As shown in Sec. 1 of ref. [7], the encoding functions $f_1(s)$ and $f_2(s)$ were chosen to form an orthonormal set $\{h(r,q;s) = \exp[i(rf_1(s) + qf_2(s))], \forall |r| + |q| \leq R/2\}$. Then, the modulated signal can be projected onto the functions $h(r,q;s)$ to obtain $P(r,q) = \langle O(s)\rangle \circ h(r,q;s)$, where the symbol $\circ$ denotes the scalar product (see Sec. 1 of ref. [7]). Thus, Eq. (9)

yields the following set of projection amplitudes from the experimental data,

$$P(1,0) \propto [U_{1ne} + U_{2ne}]^* U_{1e} \tag{10}$$

$$P(0,1) \propto [U_{1ne} + U_{2ne}]^* U_{2e} \tag{11}$$

$$P(1,-1) \propto U_{1e} U_{2e}^*. \tag{12}$$

The projections $P(1,0)$, $P(0,1)$, and $P(1,-1)$ can be directly extracted from the experimental signal $\langle O(s) \rangle$, and Eqs. (10-12) constitute a set of equations for the pathway amplitudes $U_{1ne}, U_{1e}, U_{2ne},$ and, U_{2e}. The proportionality constant is the same in Eqs. (10-12) so that ratios of projections will be free of that factor. The encoding widths $\delta\omega_1$ and $\delta\omega_2$ can be chosen so as to produce partial or full encoding of the corresponding pathways (see Section 3 of ref. [7]). For example, if we take $\delta\omega_2$ large enough such that it covers the whole width of the spectral line around ω_{43}, then we have $U_{2ne} = 0$ and $U_{2e} = U_2$. In this case, Pathway 2 is then said to be fully encoded, and using Eqs. (7, 8, 10, 11, and 12), the pathway amplitude ratio can be extracted from the experimental data as

$$F(E) \equiv |P(1,0)/P(0,1) + P(1,0)^*/P(1,-1)^*| = |U_1/U_2| \ , \tag{13}$$

Notice, from Eqs (10-12), that fully encoding both pathways (i.e $U_{1ne} = U_{2ne} = 0$) implies $P(0,1) = P(1,0) = 0$, and the only remaining nonzero projection is $P(1,-1) \propto U_1 U_2^*$. This encoding choice allows for extracting (and hence controlling) the relative phase between the two pathways, but it is insufficient to deduce their relative amplitude $|U_1/U_2|$. For controlling the amplitude ratio it is therefore necessary to partially encode one of the transitions while still fully encoding the other one. The full spectral linewidths were found in the laboratory by progressively broadening the encoding widths $\delta\omega_1,$ and $\delta\omega_2$ and extracting $P(1,0)$ and $P(0,1)$. The full linewidths are the smallest value of $\delta\omega_1$ and $\delta\omega_2$ which make $P(1,0)$ and $P(0,1)$ vanish. For Rb, the full linewidths of transitions $|1\rangle \rightarrow |2\rangle$ and $|3\rangle \rightarrow |4\rangle$ were found to be $5.2\, nm$ and $16\, nm$, respectively. The noise in the projections, κ, was estimated as the average of the absolute values of the 3rd- and 4rd-order projections (see Figure 3), as these projections should normally have a negligible value at the employed laser intensity. To avoid dividing by zero in the expression for $F(E)$ (and in $F'(E)$ below), whenever a projection amplitude in a denominator was under 3κ in magnitude, it was replaced by 3κ. Additional information may be extracted from the value of $P(0,0)$, but special

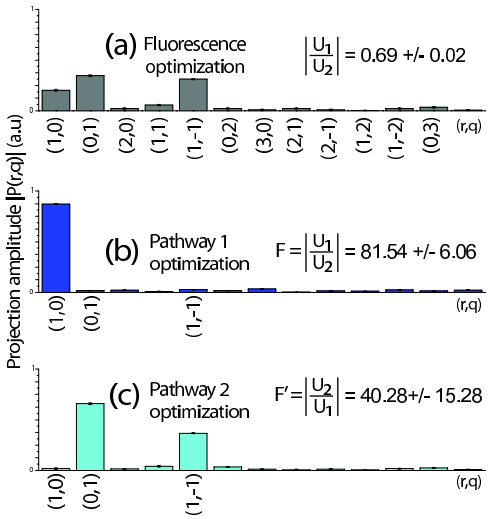

Figure 3: Projections of $\langle O(s)\rangle$ on the functions $h(r,q;s)$ for fields obtained from optimizing (a) the total fluorescence $\langle O\rangle$, (b) fitness F, (c) fitness F'.

care must be taken to compensate for signal offsets, slow drifts, etc.

In a preliminary experiment we obtained a field E_{fluo} that directly maximized the Rb fluorescence. The HE-OD projections corresponding to E_{fluo} are shown in Figure 3a, and give a ratio $F(E) = |U_1/U_2| = 0.69 \sim 1$, which implies that E_{fluo} exploits both available pathways to maximize the total fluorescence. To control the pathway ratio $F(E)$ we *inserted* HE-OD into the laboratory learning algorithm. Thus, for each candidate field $E(t)$ suggested by the algorithm, we compute $F(E)$ from the HE-OD data and seek to maximize it further on the next cycle of the loop in Figure 1. A derandomized evolutionary strategy [20] was used as the learning algorithm that varied the phase $\phi(\omega)$ to maximize $F(E)$. This experiment was also done by fully encoding pathway 1 and partially encoding pathway 2 (i.e $U_{1ne} = 0$, and $U_{1e} = U_1$), leading to a fitness $F'(E) = |P(0,1)/P(1,0) + P(0,1)^*/P(1,-1)| = |U_2/U_1|$. The results of these optimization experiments are shown in Figure 3. The field that maximizes the fitness F successfully increased the ratio to yield $|U_1/U_2| \sim 81$ (Figure 3b). The inverse was achieved by finding a field which maximized fitness F', yielding $|U_2/U_1| \sim 40$ (Figure 3c). Other fitness functions were also explored (see Sec. 2 of ref. [7]). No attempt was made to assess the Pareto competition of signals such as $\langle O\rangle$ and F, although HE-OD permits such experimental exploration.

In conclusion, we have shown how to manipulate quantum pathway amplitudes by incorporating HE-OD into a

closed-loop learning control procedure. Following the original theoretical proposal for adaptive quantum pathway control [2], the present work builds upon the original experimental implementation [5] and an advanced encoding-decoding [7] that enables a fast-throughput experimental implementation of HE-OD. The simplicity and generality of this technique make it a readily applicable and important tool for identifying control mechanisms and for utilizing the information on the fly to redirect the dynamics down desired pathways. Here we chose to manipulate the absolute value of pathway amplitude ratios, but it is also possible to manipulate the relative phases among pathways by optimizing a suitable function of the projections. Note that for the particular case of the Rb system we may eliminate a pathway by totally blocking its associated spectral components, but this method of canceling a pathway is not generally available (e.g., it is not possible when there is no clear isolated resonant frequency to block), while the HE-OD technique can be more generally applied to achieve a variety of goals. Depending on the objective, there is wide flexibility in encoding the field. For instance, the entire field may be encoded with a single function as $E_s(t) = e^{if(s)} \times E(t)$, and decoding the resulting modulated signal would give information on the pathway orders present in the dynamics. It may then be possible to maximize the amplitude of only one or multiple selected pathway orders. As another example, in the presence of many pathways it is possible to use HE-OD for seeking redirection of all the dynamics to one pathway. This goal may be addressed, providing that the desired pathway contains a transition frequency far from the frequencies involved in the other pathways, by partially encoding the desired pathway with $f_1(s)$, and fully encoding all of the other pathways with the function $f_2(s)$. Then, maximizing the fitness function $F(E) = |P(1,0)| - \sum_n |P(0,n)|$ aims to achieve the desired result, without seeking detailed information about the other pathways during the course of the optimization. Some circumstances also may benefit from employing a carrier wave stabilized laser. The ability to extract selected amounts of information at a correspondingly reduced experimental cost (i.e. with fewer measurements) is important for high-duty-cycle closed-loop quantum control. HE-OD can also be employed to analyze general N-level quantum systems [6]. Additionally, the capability of measuring quantum pathway amplitudes has important applications to Hamiltonian identification [21, 22], as the amplitudes are sensitive to the coupling matrix elements. With knowledge of the input field, measuring the pathway amplitudes can then enable the estimation of these elements.

The authors would like to thank NSF, Lockheed Martin, and the US Army Research Office under Grant number W911NF-08-1-0124 for their support. ZL acknowledges support from Fi3M and from ANR, Project Jeunes Chercheurs EPOQ2 number ANR-09-JCJC-0070.

References

[1] W. Warren, H. Rabitz, and M. Dahleh, Science **259**, 1581 (1993).

[2] A. Mitra and H. Rabitz, Phys. Rev. A **67**, 33407 (2003).

[3] A. Mitra and H. Rabitz, J. Chem. Phys. **125**, 194107 (2006).

[4] A. Mitra and H. Rabitz, J. Chem. Phys. **128**, 044112 (2008).

[5] R. Rey-de Castro and H. Rabitz, Phys. Rev. A **81**, 63422 (2010).

[6] R. Rey-de Castro, R. Cabrera, D. Bondar, and H. Rabitz, New J. Phys. **15**, 025032 (2013).

[7] See Supplemental Material at .

[8] K. Hoki and P. Brumer, Phys. Rev. Lett. **95**, 168305 (2005).

[9] C. Daniel *et al.*, Science **299**, 536 (2003).

[10] L. Pesce *et al.*, J. Chem. Phys. **114**, 1259 (2001).

[11] B. Pearson and P. Bucksbaum, Phys. Rev. Lett. **92**, 243003 (2004).

[12] T. Weinacht *et al.*, Chem. Phys. Lett. **344**, 333 (2001).

[13] F. Langhojer, D. Cardoza, M. Baertschy, and T. Weinacht, J. Chem. Phys. **122**, 014102 (2005).

[14] D. Cardoza, C. Trallero-Herrero, F. Langhojer, H. Rabitz, and T. Weinacht, J. Chem. Phys. **122**, 124306 (2005).

[15] D. Cardoza, M. Baertschy, and T. Weinacht, Chem. Phys. Lett. **411**, 311 (2005).

[16] D. Cardoza, M. Baertschy, and T. Weinacht, J. Chem. Phys. **123**, 074315 (2005).

[17] D. G. Kuroda, C. P. Singh, Z. Peng, and V. D. Kleiman, Science **326**, 263 (2009).

[18] J. White, B. Pearson, and P. Bucksbaum, J. Phys. B **37**, L399 (2004).

[19] R. Bartels, M. Murnane, H. Kapteyn, I. Christov, and H. Rabitz, Phys. Rev. A **70**, 43404 (2004).

[20] N. Hansen and A. Ostermeier, IEEE Trans. Evol. Comput. **9**, 159 (2001).

[21] J. M. Geremia and H. Rabitz, Phys. Rev. Lett. **89**, 263902 (2002).

[22] Z. Leghtas, G. Turinici, P. Rouchon, and H. Rabitz, Submitted. Preliminary version: arXiv:1102.2717v1 [quant-ph] (2011).